International Journal of Material and Mechanical Engineering, 2012, 1: 32-37
Published Online May 2012

www.ijm-me.org

Thermal Stress Measurement and Modeling in Plasma Spray Deposits Used for Attaching Fiber Optic Sensors

Amanda Krause[1], Gary Pickrell[1], Neal Pfeiffenberger[1], Robert Bodnar[2], and Robert Greenlaw[3]
[1]Department of Materials Science and Engineering, Virginia Tech, Blacksburg, USA
[2]Department of Geosciences, Virginia Tech, Blacksburg, USA
[3]MesoScribe Technologies, Inc., Huntington Beach, USA
Email: krause07@vt.edu

(Abstract) Plasma spray deposits of yttria-stabilized zirconia (YSZ) were tested as an attachment method for fiber optic strain sensors in power generation applications. Thermal stresses affect the adhesion lifetimes of the deposits, and therefore the lifetimes of the sensors when used in a variable temperature environment. The deposits were tested for elastic strain using Raman spectroscopy and modeled with COMSOL® Multiphysics®. Raman spectroscopy was used to compare the stress state of the deposits as-processed and after thermal loading by monitoring a shift by a monoclinic YSZ peak. The 3D model shows that the thermal stresses retained after the thermal load are not sufficient to cause delamination. The thermal stresses at the maximum temperature, 973 K, are large enough for failure but diffusion and other non-catastrophic relaxation mechanisms are more dominant at elevated temperatures.

Keywords: Yttria-Stabilized Zirconia; Plasma Spray Coating; Raman Spectroscopy

1. INTRODUCTION

Fiber optic sensors are currently being studied and employed for use in power generation applications due to their high accuracy, low cost, and operational convenience [1,2]. Strain sensors specifically are desired to help predict failure in host materials and for process control. Smart structures have been designed to allow a distribution of sensors within steel structures to provide practically instantaneous strain information with minimum loss of structural strength [3]. However, embedment is not possible for structures currently in use and embedded sensors can be difficult to replace or repair [4-6]. Sensors can be added to any structure with little to no disruption to the existing process. This also allows the sensors to be more accessible for any necessary maintenance.

Ceramic adhesives, mechanical brackets, and thermal spray coatings have been utilized in the past for attachment in high temperature applications [4,5,7,8]. Delamination and extensive brittle cracking are prevalent in ceramic adhesives due to their thermal and mechanical material properties [8]. Mechanical brackets are easy to install at the site but require additional sample preparation, and often do not provide good contact between the host and the sensor [5,9]. Previous tests with plasma spray and other thermal spray techniques have shown that high velocity particles can cause the fibers to break [7,10]. Also, plasma spray coatings, like ceramic adhesives, commonly have a mismatch in thermal expansion with the host structure that can lead to failure. However, they provide good protection and better adhesion compared to other methods when the process is optimized [1].

Quenching and thermal stresses are significant influences on the cyclic lifetime of plasma spray coatings [11-13]. Quenching stress is developed during processing when the high velocity molten particles solidify quickly on the relatively cool substrate. This stress is dependent on the processing conditions and the thermal properties of the coating and substrate [14]. Plasma spray coatings commonly have different coefficients of thermal expansion (CTE) than the substrates and this mismatch imposes stresses during heating and cooling [15]. The residual stress, or the stress produced during processing, includes both the quenching stress and the thermal stress that develops during cooling after deposition [16]. The residual stress state for a coating can be tensile or compressive depending on the temperature profile and which stress dominates in the system [17,18].

Thermal loading will continue to change the stress state throughout the lifetime of the coating. Coatings commonly experience tension during heating and compression during cooling at regions close to the substrate-coating interface [15]. Stresses can be relieved due to dislocation and point defect motion at elevated temperatures. Therefore, the stresses developed during heating are considered to be inconsequential to the lifetime of the coating. During cooling, diffusion is no longer thermodynamically favorable and other relaxation

mechanisms such as delamination and cracking become dominant [19-21]. These stresses need to be understood to determine the thermal life cycle of the coatings.

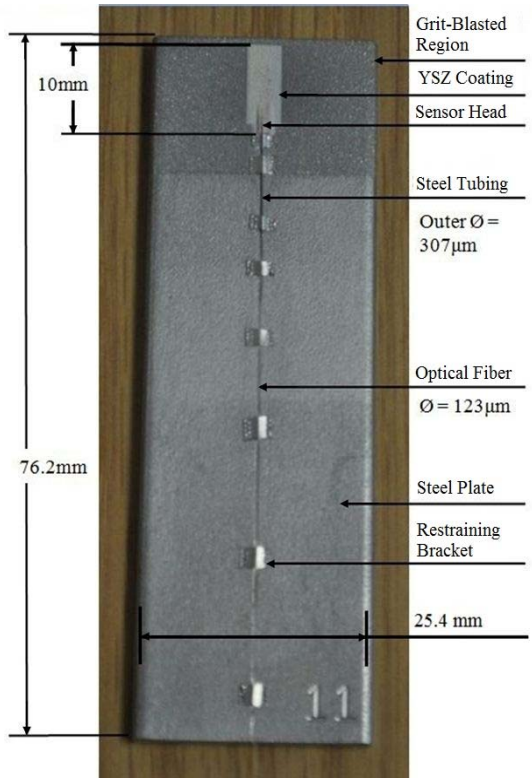

Figure 1. Labeled image of a coated fiber optic sensor.

Lattice strain can be measured by a few different non-destructive techniques including X-ray diffraction and Raman spectroscopy [13,15,17,22-24]. X-ray diffraction has a limited lateral resolution and cannot be used to determine any differences in stress state across the thickness of coatings [22]. Raman spectroscopy has been used to determine the residual stress and thermal stresses in YSZ plasma spray coatings. Finite Element Analysis can be used to model the stress distribution during heating and cooling to fully understand the changes in the system [25].

Silica optical fibers with an intrinsic Fabry-Perot interferometric (IFPI) sensing head were manufactured at Virginia Tech. The sensors can detect strain at elevated temperatures up to about 700°C depending upon the environmental conditions and can be used for process control data acquisition in power generation facilities such as coal-fired boilers. MesoScribe Technologies, Inc. produced unique coatings called MesoPlasma™ deposits to attach the fiber optic sensors to steel substrates. Yttria stabilized (8wt%) zirconia (YSZ) was selected as one of the attachment materials to study due to its desirable thermal and corrosion resistance properties [12]. Previous research has documented the effect of processing parameters and thermal history on the stress state and lifetime of plasma spray coatings [11,14,15,18,26]. This paper summarizes the effects of thermal loading on the attachment of fiber optic strain sensors for potential use in power generation applications.

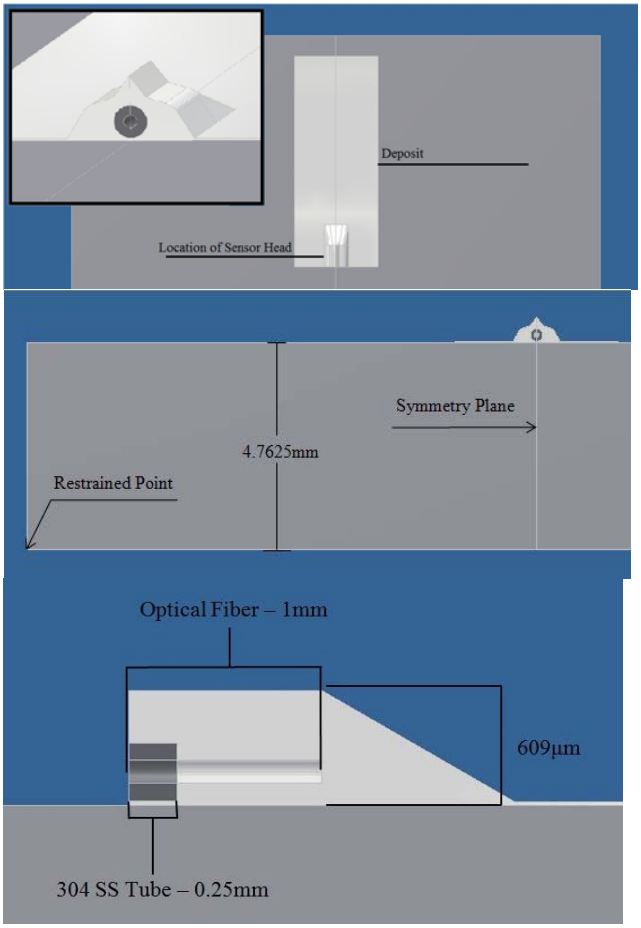

Figure 2. CAD for MesoPlasma™ deposit made in Autodesk® Inventor® that was imported into COMSOL® Multiphysics®.

2. MATERIALS AND METHODS

2.1. Sample Acquisition

The samples tested were produced by a collaborative effort between the Center of Photonic Technology at Virginia Tech and MesoScribe Technologies, Inc. The fiber optic sensors were created at Virginia Tech and then shipped to MesoScribe Technologies, Inc. for the deposition. The deposits and encapsulated fibers were analyzed at Virginia Tech in the Materials Science and Engineering, Electrical and Computer Engineering, and Geosciences Departments.

Small brackets were attached along the length of the fiber to hold it in place during processing. A 303 stainless steel substrate was used because it is a relatively common metal for structural components in power generation. The fiber was restrained and protected with a 304 stainless steel tube near the sensor head. **Figure 1** is a labeled image of a sensor. The deposit is not a uniform thickness and the geometry can be seen in **Figure 2**.

2.2.Raman Spectroscopic Analysis

Raman analyses were conducted using a JY Horiba LabRam HR800 unit in the Vibrational Spectroscopy Laboratory at Virginia Tech. The system is equipped with a 514.32nm Laser Physics 100S-514 argon laser excitation source and a 2400 grooves/mm grating. The spectra were analyzed using LabSpec-Spectrum software.

Table 1. The boundary conditions for the COMSOL® model

Study		Stationary	Time Dependent
Convective Cooling	Heat Transfer Coefficient, $W/(m^2 \cdot K)$	5	5
	Temperature, K	973	$973-5/60 \cdot t$, $t < 8{,}100$ s 287, $t \geq 8{,}100$ s
Heat Transfer in Solids and Solid Mechanics	Initial Temperature, K	298	Solution from Stationary Study
	Initial Strain, m/m	0	
	Strain-Reference Temperature, K	298	298
Time	Sequence, s	-	23,100
	Step, s	-	10

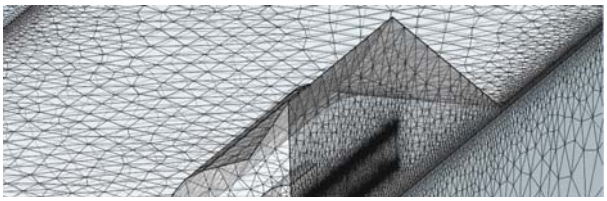

The YSZ deposits used to encapsulate the fiber optic sensors were analyzed by Raman spectroscopy to determine the change in stress state resulting from a thermal load. Fifteen different locations (five locations across the width at three different distances from the deposit-substrate interface) were tested on the cross-sections of an as-processed sample and a heat-treated sample. The heat-treated sample was heated in steps of 100k to 973K at 5K/min. After each heating step, the furnace temperature was held for 10 minutes. The furnace was then cooled to room temperature at a maximum rate of -5K/min. The cross-sections were prepared by cutting the samples using a low speed saw with an alumina abrasive steel blade. They were mounted in EpoxiCure®, a room temperature-curing epoxy, and polished to a finish of 1μm with alumina according to standard polishing techniques. Each spectrum was collected within a spectral window ranging from 100-600cm^{-1} for either 45 or 60 sec of acquisition time depending on the maximum intensity of the signal. The working distance for each sample was 4.0mm.

The spectra at five different locations across the surface of a YSZ deposit were collected before and after the sample underwent heat-treatment. The heat treatment was the same as used on the cross sectioned sample reported above. Each spectrum was collected over the spectral range 100-600cm^{-1} with either an acquisition time of 30 or 15 seconds depending on maximum signal intensity.

Table 2. The material property input data for all components.

Material	Heat Capacity, J/(kg·K)	Density, kg/m^3	Young's Modulus, GPa	Poisson's Ratio
303 SS (Substrate)[1]	500	7810	190	.33
304 SS (Tubing)[1]	500	8000	200	.29
Silica (Fiber)[2]	703	2203	73.1	.17
YSZ (Coating)[3]	480	5400	222	.3

Table 3. Temperature dependent functions for CTE and thermal conductivity of the components.

Material	Coefficient of Thermal Expansion, 1/K	Thermal Conductivity, W/(m·K)
303 SS[1]	$1.34x10^{-14} \cdot T^3 + 1.04x10^{-11} + 17.6x10^{-6}$	$3.11x10^{-6} \cdot T^2 + 9.69x10^{-3} \cdot T + 12.2$

2.3.Modeling

A 3D drawing was created on Autodesk® Inventor® and then imported into COMSOL® Multiphysics® 4.2a for analysis. The 3D model, seen in **Figure 2**, has the same dimensions as the samples. The heat transfer in solids and solid mechanics modules were utilized in COMSOL® to apply a thermal load and then analyze the von Mises stress due to the CTE differences between the components. All boundaries were free to move except the point labeled "Restrained Point" in **Figure 2**, which was a fixed point boundary condition. The 3D CAD model was split in half (parallel to the fiber) and a symmetric boundary was applied to reduce computer memory and minimize the amount of time to achieve a solution. The initial temperature for the entire system was set to 298 K. A stationary solver was used to solve for the stresses at 973 K. The temperature was set by applying convective cooling to all exterior faces of the geometry except the cross section of the fiber, shown in **Figure 2**. The heat transfer coefficient for air was set to 5 $W/(m^2 \cdot K)$. The stationary solution was used as the initial stress state for a time-dependent study, which ramped down the temperature from 973 K to 298 K using convective

cooling with a time dependent function at a rate of -5K/min. The system was solved every 10 seconds for a time sequence of 23,100 seconds. Although the air was cooled to room temperature in 8,100 seconds according to the input temperature function, the entire part required a longer time to cool to 298 K. All of the boundary conditions can be found in **Table 1**.

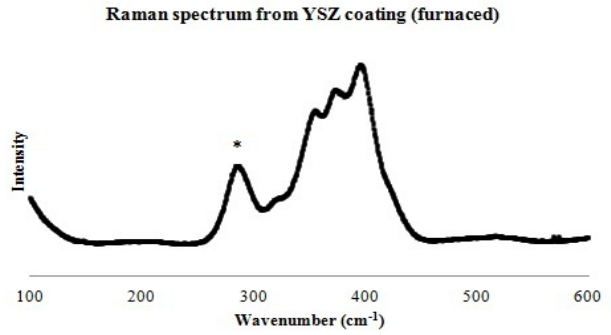

Figure 4. Typical Raman spectrum produced for a YSZ deposit.

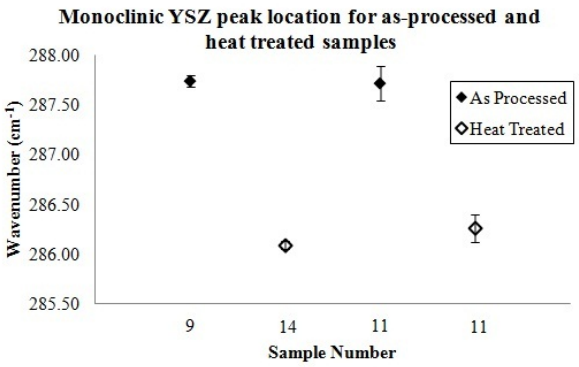

Figure 5. Comparison of peak locations for as-processed and heat treated YSZ samples.

The material properties for each component were determined from data reported in the literature and then fitted in Wolfram Mathematica® 8 to develop temperature dependent functions for CTE and thermal conductivity. All material properties that are independent of temperature can be found in **Table 2**. The CTE and thermal conductivity data for the YSZ coating was based on the temperature dependent data on a YSZ plasma spray coating of the same composition and similar density [27]. The material properties as functions of temperature can be found in **Table 3**.

The heat transfer in solids module requires the thermal conductivity to calculate the temperature of the system resulting from convective cooling. Therefore, the material properties are functions of a user input temperature that is a function of time. The input temperature function was determined from a model run with constant thermal properties to determine how fast the components cool. The function is listed at the bottom of **Table 3**.

The system was meshed using tetragonal elements, which were distributed more finely along the edge boundaries of the components, as seen in **Figure 3**.The total system contained 514522 elements and the system was solved for 2991036 degrees of freedom.

3. RESULTS

3.1.Raman Spectra for YSZ Coatings

The Raman spectra were fitted using the Lorentzian function with five peaks selected in the 200-500cm^{-1} range as seen in **Figure 4**. The peaks observed have been previously reported for the monoclinic and tetragonal phases [17,23,24]. All fitted peak positions were recorded for each spectrum. The data retrieved for both cross-sectioned samples showed no consistent peak shift across the thickness or width of the individual deposits. However, a noticeable peak shift was observed between as-processed samples and samples that were heat-treated as seen in **Figure 5**. **Figure 5** reports the peak location for the starred peak in **Figure 4** of the different samples. This peak was selected because it was well defined and showed minimum overlap with other peaks, which allowed a more accurate fit. The error bars show the 95% confidence interval for the data collected.

The peak shift was consistent for the cross-sectioned and surface tested samples. The direction of the peak shift may be indicative of an applied force in the tensile direction. The larger variance in sample 11 is due to the surface being rougher than the polished cross-sections.

3.2.COMSOL® Modeling

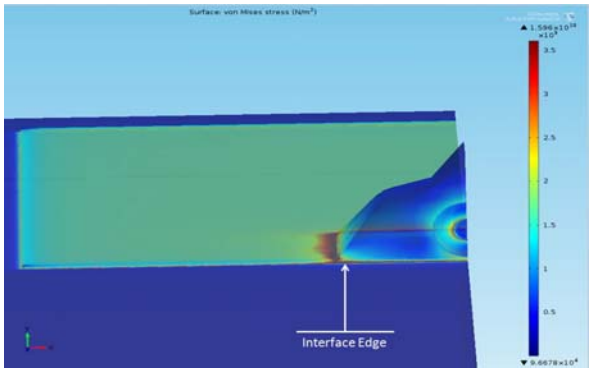

(a)

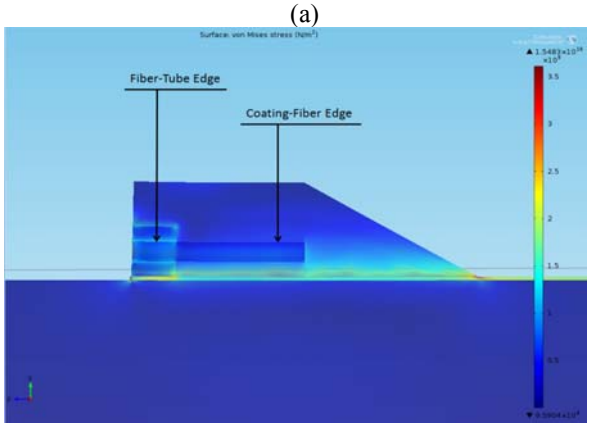

(b)

Figure 6. The COMSOL® produced stress distribution at 973K for the (a) front of the model and (b) the right side (symmetry plane) view of the model. The maximum of the color range is set to the adhesion strength of the deposit.

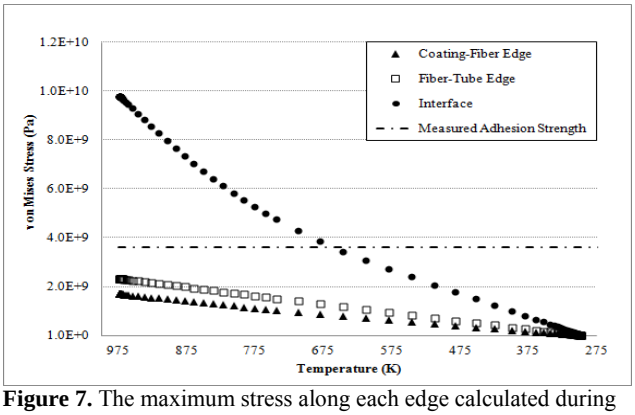

Figure 7. The maximum stress along each edge calculated during cooling

The model predicts the highest von Mises stress at 973 K along the substrate-coating interface. **Figure 6** shows the stress distribution at 973 K. Stresses represented by dark red, at this scale, would most likely fail according to a previous adhesion strength test, which is not discussed here. The samples analyzed by Raman spectroscopy that were heat-treated did not show any evidence of catastrophic failure.

Figure 7 shows the stress behavior of three different edges (interface edge, fiber-tube edge, coating-fiber edge) shown in **Figure 6 (a) and (b)**, as a function of temperature and the measured adhesion strength at room temperature. The reported stress at each temperature is the maximum stress along the entire edge. The stress along the fiber edge, either at the fiber-coating interface or the fiber-tubing interface, never reaches stress sufficiently high to cause failure under these conditions. The edge at the fiber-tubing interface experiences a higher absolute stress than the fiber-coating interface at all temperatures.

4. DISCUSSION

4.1.Raman Analysis of Plasma Sprayed Coating

In-situ stress Raman studies of tetragonal YSZ coatings show a peak shift to lower wavenumbers during the application of a tensile force. The YSZ peak commonly analyzed for stress, located approximately at 640cm^{-1}, is not well defined in the collected spectra and cannot be used in this assessment [17,23,24]. The monoclinic peaks are more dominant and easily fitted for analysis but have not been previously documented with this technique. The deposit in interpreted to have experienced a tensile force if the monoclinic peak recorded at ≈287cm^{-1} follows the same trend as the tetragonal peaks. Because the initial stress state is not known, the deposit could be relaxing to a less compressive state or to a tensile state.

Teixeira et al. reported that subsequent heat treatments add a compressive force for YSZ coatings due stresses induced during cooling [15]. Because the deposits report a stress shift in the tensile direction, the compressive forces must have been relaxed at room temperature or were subordinate to relaxation and tensile forces at elevated temperatures. The samples did not exhibit delamination or cracking at room temperature, which would have alleviated any compressive forces induced during cooling.

The compressive forces during cooling were not large enough to counteract the relaxation mechanisms at elevated temperatures, which were more efficient due to the geometric shape and the inclusion of the embedded fiber [30,31]. Point defect and dislocation movement to both the fiber cavity and out of the surface of the deposit may allow for a more extensive relaxation at elevated temperatures than was observed in the pure, flat and semi-infinite coatings. If the relaxation is more dominant than the compressive force caused during cooling, the samples will report a stress shift in the tensile direction. The samples should be tested under conditions of continuous thermal cycling to see if there is any change in the stress direction over time and if the stress behavior improves the lifetime of the deposit.

4.2.COMSOL® Modeling

The highest stress regions are located at the interfaces between the components. Delamination and cracking at these regions will be detrimental to the strain transfer fidelity and make the sensors unreliable. However, the model shows that the system experiences failure-inducing stresses only at temperatures above 650K. At elevated temperatures, these stresses may be reduced by point defect and dislocation movement. Surface diffusion is believed to occur at low temperatures because it requires a smaller activation energy than volume and grain boundary diffusion [31]. The unique geometry of the deposits and the void introduced from the fiber may provide the system with a large driving force for diffusion to relax the system enough to prevent catastrophic failure. This agrees with the Raman spectroscopic analyses that suggest that relaxation mechanisms are highly active at elevated temperatures.

The tubing around the fiber serves to protect and restrain the fiber during processing. The stress model shows that the fiber experiences a larger stress at the fiber-tubing interface compared to the coating-fiber interface. The tubing has a higher CTE than the silica fiber and the coating, which increases the absolute stress in this region. The stress at the substrate-coating interface is the greatest and will be the limiting factor for the sensor's cyclic lifetime. However, any discontinuous strain along the fiber may cause micro-bending that will add interference in the signal. The tubing material and length may need to be optimized to allow for protection during processing and not interfere during strain data acquisition.

5. CONCLUSION

The MesoPlasma™ deposits were tested to determine the change in stress state and if catastrohpic failure would occur from a thermal load. Raman spectroscopic data and theoretical calculations suggest that non-destructive relaxation

mechanisms are active at high temperatures and that the induced stresses during cooling do not cause catastrophic failure. The steel tubing protected the fiber during processing but under thermal loading it adds a higher stress concentration around the fiber. The tubing will not influence the sensor's cyclic lifetime though since the deposit will most likely fail first at the substrate-coating interface. Future testing should determine the change in stress after continuous thermal cycling and if the material system can be optimized.

6. ACKNOWLEDGEMENTS

The authors would like to thank and acknowledge the funding for this work from DOE under contract number DE-SC0001017 and MesoScribe Technologies, Inc. for their participation in this project.

REFERENCES

[1] E. Udd, Fiber optic smart structures, Wiley, New York, (1995)
[2] H.-N. Li, D.-S. Li, and G.-B. Song, Eng. Struct. 3, 11, (2003)
[3] G.J. Knowles, Editor. ADPA AIAA ASME Spie Conference on Active Materials and Adaptive Structures, (1991) November 4-8; Alexandria, United States.
[4] N. Narendran and J.M. Weiss, Field Mountable Fiber Optic Sensor. U.S. Patent 5 594 819, July 31 (1997)
[5] E. Udd and D. Inaudi, Editors. Smart Structures and Materials 2005: Smart Sensor Technology and Measurement Systems, (2005) May 16; San Diego, United States.
[6] M. Farshad, Sci. Iran. 2, 1, (1995)
[7] K.C. Kelley, Ceramic Adhesive. U.S. Patent 5 468 290, Nov 21 (1995).
[8] V.K. Varadan, Editor. Smart Structures and Materials 1993: Smart Materials, (1993) February 2; Albuquerque, United States.
[9] W.R. Habel and A. Bismarck, J. Struct. Contr. 7, 1, (2000)
[10] Z. Zhao, Editor. International Photonics and Optoelectronics Meetings, (2009) August 14-16; Wuhan, China.
[11] S. Kuroda and T.W. Clyne, Thin Solid Films. 200, 1, (1991)
[12] J.R. Davis, Handbook of thermal spray technology, ASM International, Materials Park, (2004)
[13] M. Levit, I. Grimberg, and B.Z. Weiss, Mat. Sci. Eng. A-Struct. 206 1, (1996)
[14] T.F. Bernecki, Editor. Thermal spray coatings : properties, processes, and applications: proceedings of the Fourth National Thermal Spray Conference, (1991) May 4-10; Pittsburgh, United States.
[15] V. Teixeira, M. Andritschky, W. Fischer, H.P. Buchkremer, and D. Stover, Surf. Coat. Tech. 120-121, (1999)
[16] O. Kesler, M. Finot, S. Suresh, and S. Sampath, Acta. Mater. 45, 8, (1997)
[17] V. Teixeira, M. Andritschky, W. Fischer, H.P.Buchkremer, and D. Stover, J. Mater. Process. Tech. 92-93, (1999)
[18] J. Matejicek, S. Sampath, P.C. Brand, and H.J. Prask, Acta. Mater. 47, 2, (1999)
[19] R.A. Miller and C.E. Lowell, Thin Solid Films. 95, 3, (1982)
[20] P. Robin, F. Gitzhofer, P. Fauchais, and M. Boulos, J. Therm. Spray. Techn. 19, 5, (2010)
[21] W.A. Jesser, S. Afr. J. Sci. 104, (2008)
[22] J. Matejicek, S. Sampath, and J. Dubsky, J. Therm. Spray. Techn. 7, 4, (1998)
[23] J. Cai, Appl. Phys. Lett. 62, 22, (1993).
[24] T. Tomimatsu, Y. Kagawa, and S.J. Zhu, Metall. Mater. Trans. A. 34, 8, (2003)
[25] S. Gill and T. Clyne, Metall. Mater. Trans. B. 21, 2, (1990)
[26] S. Sampath and H. Herman, J. Therm. Spray. Techn. 5, 4, (1996)
[27] L. Pawlowski, D. Lombard, and P. Fauchais, J. Vac. Sci. Technol. A. 3, 6, (1985)
[28] D.O. Kipp, Metal Material Data Sheets, MatWeb - Division of Automation Creation, Inc,(2010). Online version available at: http://www.knovel.com.ezproxy.lib.vt.edu:8080/web/portal/browse/display?_EXT_KNOVEL_DISPLAY_bookid=3422&VerticalID=0.
[29] N.P. Bansal and R.H. Doremus, Handbook of glass properties, Academic Press, Orlando, (1986)
[30] G.L. Povirk, A. Needleman, and S.R. Nutt, Mater. Sci. eng. A. 125, 2, (1990)
[31] G. Cao and Y. Wang, Nanostructures & nanomaterials : synthesis, properties, and applications, Imperial College Press, London, (2011)